Title
Deconvolution Reveals the Activity of Specific Glycan Forms

Author
Tsao, Amanda J

Publication Date
2021

Peer reviewed|Thesis/dissertation

UNIVERSITY OF CALIFORNIA

Los Angeles

Deconvolution Reveals the Activity of Specific Glycan Forms

A thesis submitted in partial satisfaction

of the requirements for the degree Master of Science

in Bioinformatics

by

Amanda Jayne Tsao

2021

ABSTRACT OF THE THESIS

Deconvolution Reveals the Activity

of Specific Glycan Forms

by

Amanda Jayne Tsao

Master of Science in Bioinformatics

University of California, Los Angeles, 2021

Professor Aaron S. Meyer, Chair

The ability of Fcγ receptors to bind antibodies and induce responses such as antibody-dependent cellular cytotoxicity (ADCC) can impact disease outcomes. FcγR binding is known to be regulated by modification of glycans located in the Fc domain of IgG, although the influence of specific glycans on binding and subsequent activation remains relatively unknown. Glycan-engineering has been previously used to study the effects of different glycans on Fc-mediated responses, but even extensive glycan-engineering methods are limited in their ability to create antibodies expressing a single, pure glycan. In this paper, we apply deconvolution to identify the contributions of individual glycans to FcγR binding and ADCC. Deconvolution revealed that afucosylated glycans are associated with increased ADCC activity and increased binding affinity to FcγRIIIa and FcγRIIIb. Additionally, FcγRIIIa-158F exhibited higher binding activity than

FcγRIIIa-158V despite having similar levels of ADCC, which suggests FcγRIIIa-158F may induce ADCC more efficiently. The deconvolution methods we present can be applied in the future to other responses mediated by Fcγ receptors such as complement activation.

The thesis of Amanda Jayne Tsao is approved.

Matteo Pellegrini

Van Maurice Savage

Aaron S. Meyer, Committee Chair

University of California, Los Angeles

2021

Table of Contents

List of Figures

Acknowledgements

Foremost, I would like to express my sincere appreciation to my advisor, Dr. Aaron Meyer, for his invaluable guidance and feedback through the research and writing of this thesis. I would also like to thank my lab teammates, Sumedha Kanthamneni and Eva Hunter, for their essential contributions to this project. Last but not least, I wish to thank my parents for their love and support through every step of my academic and personal growth.

INTRODUCTION

Despite existing knowledge about the influence of human immunoglobulin G (IgG) on Fc gamma receptors (FcγR) and complement activation, the influence of specific IgG1 glycans on binding and subsequent activation remains relatively unknown. In general, FcγRs have a low affinity for IgGs unless they are a part of a multimeric immune complex [Duchemin et al., 1994]. FcγRI is the exception, as it can interact with monomeric IgGs with high affinity [Bournazos et al., 2020a]. FcγR-mediated effector functions are highly complex and variable. Therefore, deeper understanding of how to influence receptor binding and downstream effector functions has the potential to optimize efficacy of cellular response, increase therapeutic potency, and minimize inappropriate activation.

When FcγRs on immune cells interact with an immune complex or an opsonized cell generated by a pathogenic trigger, the FcγRs crosslink, which leads to the activation of the immunoreceptor tyrosine-based activation motif (ITAM) domains. The subsequent signaling cascade can result in antibody-dependent cellular phagocytosis (ADCP) of the complex or cell detected, along with the release of pro-inflammatory cytokines. Additionally, the FcγR-mediated response can also activate innate effector cells and trigger cell death through antibody-dependent cellular cytotoxicity (ADCC), which can help fight diseases such as infections and cancer [Von Holle & Moody, 2019; Zahavi et al., 2018]. Natural killer (NK) cells are the most important contributors to ADCC and are the only cell type that almost solely expresses FcγRIIIa [van Erp et al., 2019; Dekkers et al., 2017]. The degree of ITAM domain activation is modulated by the antagonist response of FcγRIIb, preventing excessive or inappropriate cellular responses [Bournazos et al., 2020b].

FcγRs are a class of surface proteins found on immune cells, which are known to have strong impacts in immune modulation within the body. There are three major types of FcγRs: FcγRI, FcγRII, and FcγRIII, each of which is known to have either an activating or inhibiting effect. This depends on the presence of previously mentioned ITAMs as well as immunoreceptor tyrosine-based inhibitory motifs (ITIMs) on the intracellular domain. The general effects of different FcγRs are known to some extent. FcγRI, FcγRIIa, FcγRIIc, and FcγRIIIa are activating due to ITAM presence, while FcγRIIb has an inhibitory effect due to the presence of ITIMs. FcγRIIIb contains a GPI-anchored protein and therefore its binding does not activate signal transduction, but rather transduces activation by crosslinking with other activating FcγRs. It is also known that the surface expression of these receptors on immune cells can be modulated by the presence of various cytokines and anti-inflammatory or pro-inflammatory signaling [Bournazos et al., 2020a]. The response generated by FcγR activation depends on the net contribution from activating and inhibitory signals.

One regulatory mechanism for FcγR binding is modification of the glycans located in the Fc domain of IgG. This type of modification leads to changes in the interaction between a glycan at position 162 in human FcγRIIIa or FcγRIIIb and the Fc glycan on IgG [Li et al., 2017]. The binding patterns derived from glycan modifications can impact the disease outcomes of autoimmune and alloimmune disorders. To investigate the relationships between glycan modifications, FcγR binding, complement activation, and FcγR-mediated cellular response, researchers at the University of Amsterdam used glycan-engineering to create mixtures of IgG1 with varied amounts of distinct glycans. The 24 individual glycans had different profiles of bisection, fucosylation, galactosylation, and sialylation at asparagine 297 (Asn297) within the Fc domain of IgG1. The mixtures contained known combinations of the individual glycans, and

their binding affinities were recorded for each type of FcγR, compared to the mean affinity of unmodified IgG1. The largest changes were observed in IgG1 binding to FcγRIIa-158F, FcγRIIIa-158V, FcγRIIIb-NA1, and FcγRIIIb-NA2. Furthermore, ADCC activities of the modified IgG mixtures were measured using NK cells from FcγRIIIa-158F/F and FcγRIIIa-158V/V donors. This yielded more information about glycan influence on receptor binding and cell death. However, the contributions of individual glycans were not given by the data collected because pure glycans are very difficult to isolate experimentally [Dekkers et al., 2017]. When experimental methods such as glycan-engineering pose significant challenges, computational approaches are often useful to help improve our understanding of the complex mechanisms at hand.

A computational technique called deconvolution is used to process data that have undergone an undesired convolution [Smith, 1997]. Deconvolution aims to recover the signal that would have been measured in the absence of convolution [Smith, 1997]. Mathematically, we want to find the solution f, given the convolution function g and measured signal h:

$$h = f * g$$

For deconvolution to produce good results, it is often necessary to know the convolution function or be able to accurately estimate it [Smith, 1997]. When the convolution is unknown, blind deconvolution can be attempted. However, blind deconvolution algorithms are more complex and often fail to produce the desired results [Levin et al., 2009].

Deconvolution has been applied extensively in seismology, imaging, and absorption spectra to process signals. It has also been used to study complex molecular systems to determine the activities of individual species within mixtures. For example, Proteolytic Activity Matrix Analysis (PrAMA) infers the activities of individual enzymes within mixtures of many proteases

[Miller et al., 2011]. Similarly, MUlti-Subject SIngle Cell deconvolution (MuSiC) estimates cell type proportions from bulk RNA-seq data containing several different cell types [Wang et al., 2019]. In these cases, the undesired convolution is the combination of individual species (enzymes and cell types, respectively) to form mixtures and the desired results are the deconvolved measurements of those species in isolation. While deconvolution has been applied to several topics in biology, it has not yet been utilized to profile Fc glycan activity. This is an especially useful application of deconvolution due to the difficulty of isolating Fc glycans experimentally.

Currently, glycan-engineering methods are limited in their ability to create antibodies expressing a single, pure glycan. Even combining several glycan-engineering methods yields mixtures of glycan forms [Dekkers et al., 2017]. In this paper, we apply deconvolution to identify the contributions of individual glycans to Fc binding and immune response. Deconvolution was performed on the glycan matrix (Table 2), receptor binding (Figure 8), and ADCC data (Figure 9). This allowed us to infer the properties of the pure glycan species, which contribute to Fc binding in unique ways. Understanding these contributions is important for creating immune therapies that target Fc-mediated responses. However, because these responses are difficult to study experimentally, they are not well understood and remain underutilized in current immune therapies. Deconvolution, therefore, provides a method of analyzing glycan mixtures to improve our understanding of Fc-mediated immune response.

METHODS

Data

The data used in this study was taken from Dekkers et al., which details experiments performed on mixtures of variously glycosylated IgG1 [Dekkers et al., 2017]. Two panels of

IgG1 were prepared such that the first panel was specific for the human RhD (anti-D) antigen and the second for 2,4,6-trinitrophenyl hapten (anti-TNP) [Dekkers et al., 2017]. 20 anti-D and 20 anti-TNP mixtures were created through a combination of several glycan-engineering methods. Each mixture contained different amounts of several unique glycans, of which there were 24 in total. The varied levels of fucosylation, bisection, galactosylation, and sialylation in each mixture were also reported. Mixtures were named according to their glycan-engineering treatments (Table 2). Glycans were named according to their profiles of galactose, fucose, N-acetylglucosamine, and N-acetylneuraminic (sialic) acid (Table 1). The specific glycans present in each mixture were quantified by mass spectrometry. Then, the mixtures were profiled for their ADCC, complement activation, and receptor binding activities. We performed deconvolution on ADCC and receptor binding to obtain the individual contributions of each glycan species. ADCC data was normalized with correction for spontaneous lysis as described previously [Dekkers et al., 2017].

	G0F	G1F	G2F	G0FN	G1FN	G2FN	G1FS	G2FS	G2FS2	G1FNS	G2FNS	G2FNS2
Fucosylation	+	+	+	+	+	+	+	+	+	+	+	+
Bisection	-	-	-	+	+	+	-	-	-	+	+	+
Galactosylation	-	+	++	-	+	++	+	++	++	+	++	++
Sialylation	-	-	-	-	-	-	+	+	++	+	+	++

	G0	G1	G2	G0N	G1N	G2N	G1S	G2S	G2S2	G1NS	G2NS	G2NS2
Fucosylation	-	-	-	-	-	-	-	-	-	-	-	-
Bisection	-	-	-	+	+	+	-	-	-	+	+	+
Galactosylation	-	+	++	-	+	++	+	++	++	+	++	++
Sialylation	-	-	-	-	-	-	+	+	++	+	+	++

Table 1: Fucosylation, Bisection, Galactosylation, and Sialylation of each glycan species. Glycans were named according to number of galactoses (G), presence of a core fucose (F), presence of a bisecting N-acetylglucosamine (N), and number of N-acetylneuraminic (sialic) acids (S).

Deconvolution

Our deconvolution technique assumes that all total measured IgG1 mixture characteristics from Dekkers et al., namely ADCC, complement activation, and receptor binding activities, are a summation of the individual contributions of each glycan in the mixture. We also assume that the contribution of a single glycan to a mixture's activity is directly proportional to the fraction of glycan present in that mixture. These assumptions give the following linear model:

$$y = X\beta + \varepsilon$$

$$[y_1 \dots y_m] = \begin{bmatrix} x_{1,1} & \cdots & x_{1,n} \\ \vdots & \ddots & \vdots \\ x_{m,1} & \cdots & x_{m,n} \end{bmatrix} \begin{bmatrix} \beta_1 \\ \vdots \\ \beta_n \end{bmatrix} + \varepsilon$$

- y is the observed average mixture characteristic
- X is the m-by-n matrix with m mixture observations and n glycans
- β is a vector of n values, which indicates the contribution of each glycan to the measurement of total ADCC, receptor binding, or complement activation
- ε is the noise in the measurements

Values of X were measured and reported in Table 1 of Dekkers et al. (Table 2). For ADCC deconvolution, the values were calculated as the average of four observations per mixture for each of the 20 mixtures. For complement activation and receptor binding, values of y were directly reported in Dekkers et al. The ADCC and receptor binding experiments used the anti-D mixtures, while the complement activation experiments used the anti-TNP mixtures.

We aimed to estimate the contribution of each glycan to the experimentally observed mixture ADCC, complement activation, and receptor binding activity. While there are several solving techniques that may have been utilized, we chose to use non-negative least squares (NNLS). NNLS is a linear regression model with the additional constraint that all coefficients or

β-values must be non-negative. This suited our application because measurements of ADCC, complement activation, and receptor binding must be non-zero. Negative values indicate measurement errors and have no meaningful biological interpretation.

Bootstrapping

Bootstrapping is a statistical technique used to assess generalization to new datasets by resampling from a single body of data. These new datasets are used to fit the NNLS model and produce a distribution of model outputs. For this application, we performed a stratified resampling of the mixture data such that at least one of each mixture type would appear in the newly formed dataset. The mean measured value for each mixture in the new dataset was used to fit the NNLS model. The resultant distributions were used to calculate standard error for the predicted activity of each glycan form.

Fitting and Cross-Validation

To evaluate the fitting of the deconvolution, we performed matrix multiplication on the mixture matrix X and inferred vector β to obtain the characteristics of each mixture. These fit values were then compared to the measured values from the Dekkers et al. in grouped bar plots (Figures 3, 5).

We also performed cross-validation by sequentially removing each mixture, deconvolving the remaining 19 mixtures, and using the resulting β vector to infer the activity of each missing mixture (Figures 6, 7). These results allowed us to determine how well the deconvolution method predicts the activity of new mixtures.

RESULTS

Glycan mixtures display multivariate changes in FcγR binding and ADCC

Principal components analysis (PCA) was run using five components, which explained almost 100% of the variance in the original data (Figure 1C). Two components explained 99% of the variance. Scores using two principal components for FcγR binding and ADCC revealed that fucosylated mixtures (-G, Unmodified, +G, +G+S, +G+S+ivs, -G+B, +B, +B+G, +B+G+S, +B+G+S+ivs) were highly correlated (Figure 1A). While scores for afucosylated mixtures varied in both Components 1 and 2, there was a clear separation between galactosylated (-F+B+G, -F+G, -F+G+S, -F+G+S+ivs, -F+B+G+S, -F+B+G+S+ivs) and non-galactosylated mixtures (-F-G, -F-G+B, -F, -F+B) (Figure 1A). Loadings using two principal components showed that FcγRIIIa-158V binding is highly correlated with ADCC mediated by both FcγRIIIa-158V/V and FcγRIIIa-158F/F (Figure 1B). Bindings for FcγRIIIa-158F, FcγRIIIb-NA1, and FcγRIIIb-NA2 were also somewhat correlated with FcγRIIIa-158V binding, FcγRIIIa-158V/V ADCC, and FcγRIIIa-158F/F ADCC in component 1 (Figure 1B). These groups were less correlated in component 2, but this second component only accounts for 2% of the variance. Lastly, the loadings for both FcγRI and FcγRII binding were essentially zero in both components, which means that the variance in FcγRI and FcγRII was not explained by the first two components (Figure 1B).

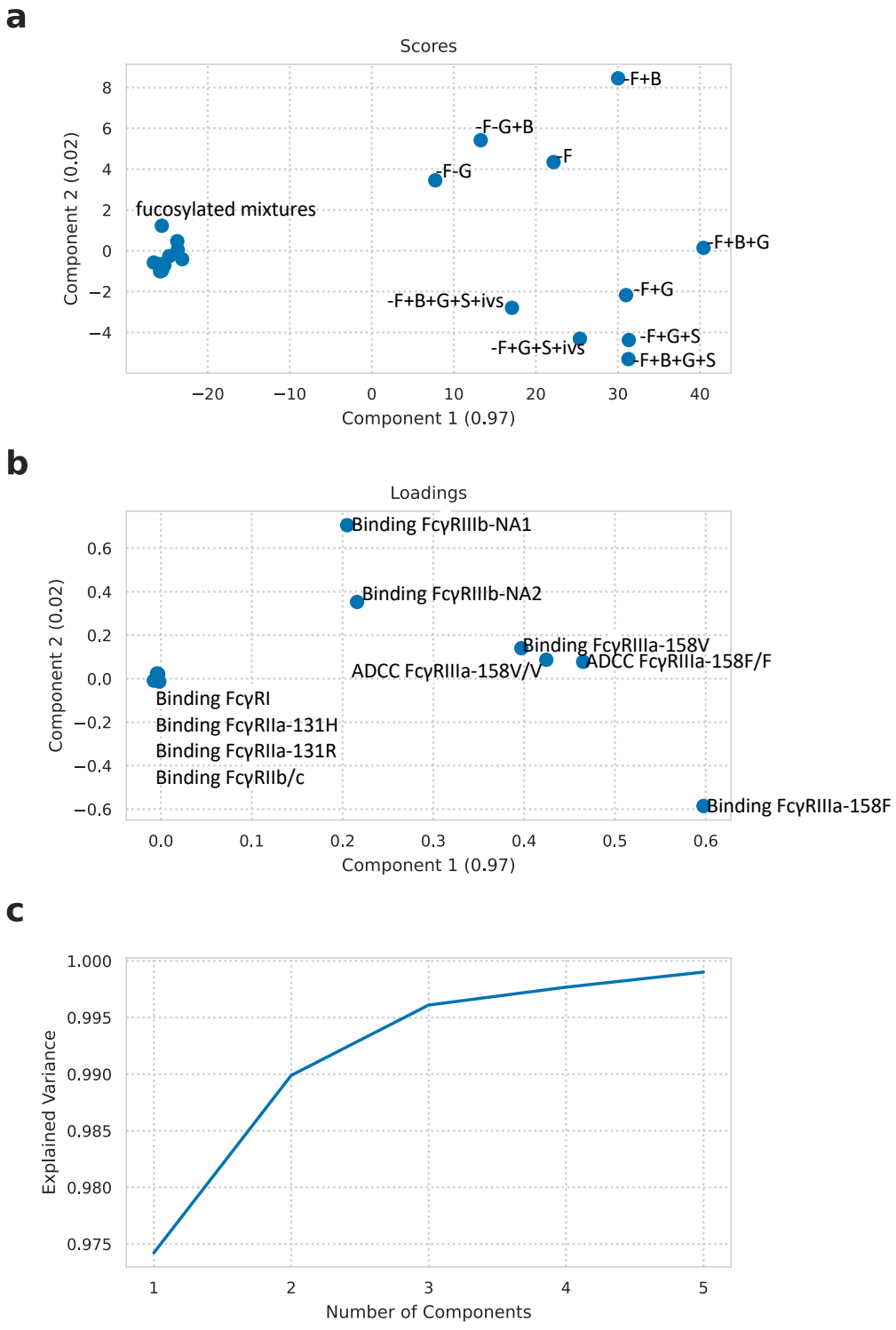

Figure 1: Principal Components Analysis of FcγR Binding and ADCC. Scores (A) and loadings (B) using two principal components, which explain 99% of the data. R2X plot indicating the percentage of variance explained by each principal component (C).

Deconvolution of ADCC

We performed deconvolution on the ADCC mixture data using NNLS. To reduce the uncertainty of the deconvolution, we decreased the degrees of freedom by assigning certain molecular species to have a shared activity, based on prior knowledge regarding the glycan features that affect ADCC. The following glycans were grouped together: G1 and G1S, G2 and G2S, G0N and G2S2, G1N and G1NS, and G2N and G2NS. The deconvolution yielded the inferred contributions of each glycan species to ADCC mediated by NK cells from FcγRIIIa-158F/F and FcγRIIIa-158V/V donors (Figure 2). The fucosylated species (G0F, G1F, G2F, G0FN, G1FN, G2FN, G1FS, G2FS, G2FS2, G1FNS, G2FNS, G2FNS2) showed no ADCC activity. Because every mixture showed some degree of ADCC activity, this result indicates that total mixture ADCC comes from the afucosylated species alone, which constitute at least a small proportion of each mixture. Of the afucosylated species (G0, G1, G2, G0N, G1N, G2N, G1S, G2S, G2S2, G1NS, G2NS, G2NS2), G1N, G2N, G1NS, and G2NS had the highest inferred activities in FcγRIIIa-158 F/F, while G2N and G2NS were the highest in FcγRIIIa-158 V/V. G2NS2 had the lowest values by far, followed by G0, G0N, and G2S2 in both FcγRIIIa-158F/F and FcγRIIIa-158V/V. Bootstrapping yielded reasonably small error bars for most of glycans, indicating relatively little uncertainty in activity among the afucosylated glycans' inferred activity.

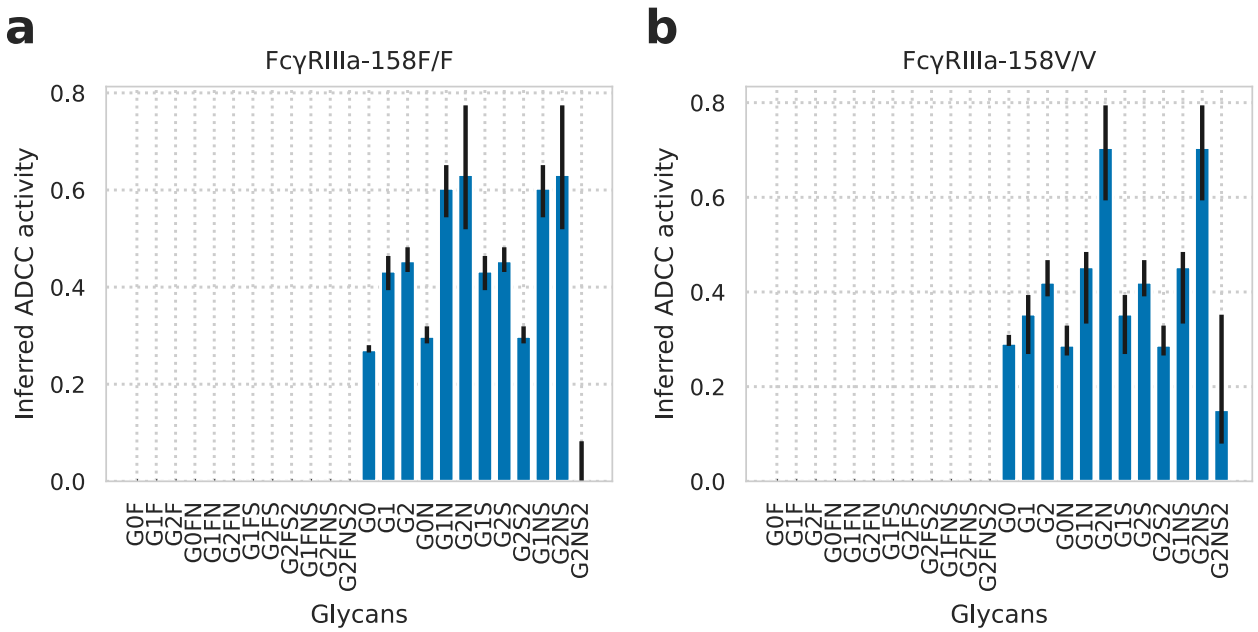

Figure 2: Deconvolution of ADCC. Inferred contributions of each pure glycan species to ADCC mediated by NK cells from monozygotic FcγRIIIa-158F/F donors (A) and FcγRIIIa-158V/V donors (B). Measurements of ADCC in glycan mixtures were taken from Dekkers et al. (Figure 9). Error bars were obtained with bootstrapping and represent the 67% confidence intervals.

To assess the fitting of the deconvolution as well as our assumptions about glycans with shared activity, we reversed the deconvolution by matrix multiplication between the mixture matrix and inferred β vector. We then compared these values with the measured ADCC data from Dekkers et al. (Figure 3). The inferred and measured values were very similar. The fucosylated mixtures showed little to no ADCC activity, whether inferred or measured. The afucosylated mixtures exhibited much higher ADCC activities in both the inferred and measured instances. This indicated that the absence of a core fucose drastically increases ADCC.

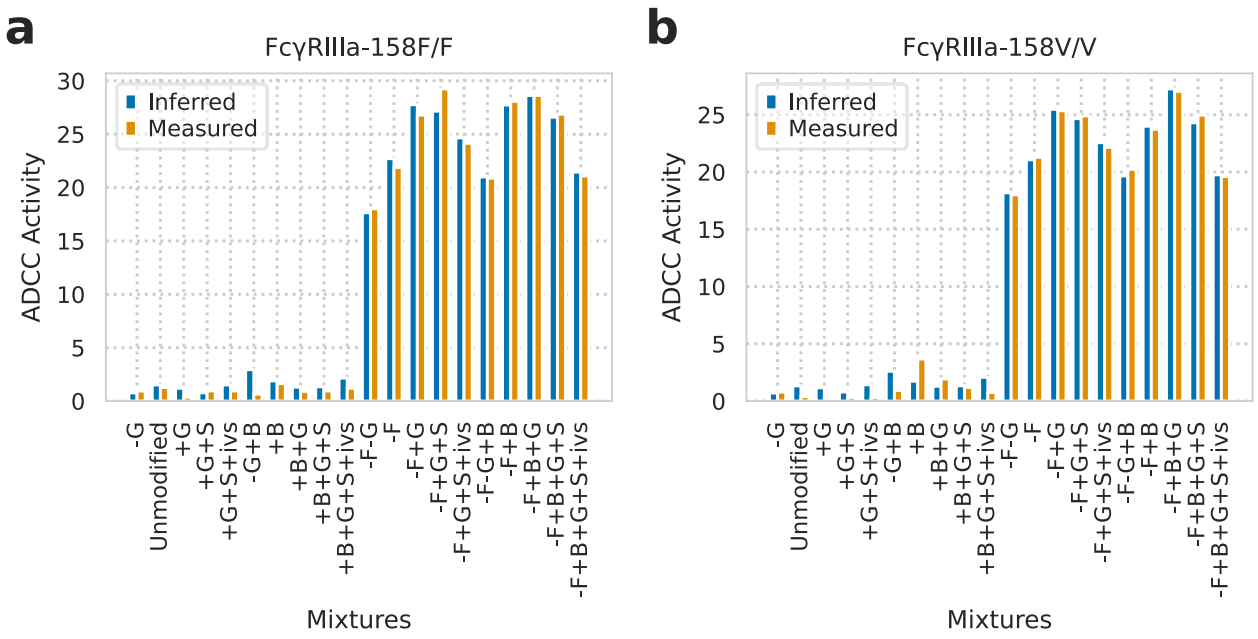

Figure 3: Fitting of measured and inferred ADCC. Grouped bar plot comparing the inferred and measured activities of 20 mixtures to ADCC mediated by NK cells from FcγRIIIa-158F/F donors (A) and FcγRIIIa-158V/V donors (B). Measured values were taken from Dekkers et al. (Figure 9). Inferred values were calculated using the previous ADCC deconvolution.

Deconvolution of Fcγ Receptor Binding

Similar to the deconvolution of ADCC, we used NNLS to deconvolve the contributions of individual glycans to receptor binding. The same shared activity assignments we used for the ADCC deconvolution were used for FcγRIIIa and FcγRIIIb binding. In addition, all FcγRI glycans were assigned to share the same binding activity. Grouping was not used for FcγRIIa and FcγRIIb/c. The inferred glycan contributions varied across different types of Fcγ receptors (Figure 4). The magnitudes of binding were lower in the FcγRI and FcγRII allotypes, compared to the FcγRIII allotypes. For the FcγRII allotypes, galactosylation and bisection increased receptor binding. G2FNS had the highest binding activity in FcγRIIb/c, while G2FN was the

highest in FcγRIIa-131R and G2NS in FcγRIIa-131H (Figure 4A-D). For FcγRIIIa-158F and FcγRIIIa-158V, the afucosylated glycans exhibited higher binding activities than the fucosylated glycans (Figure 4E-F). This result is consistent with the previous ADCC deconvolution, which used NK cells from FcγRIIIa-158F/F and FcγRIIIa-158V/V donors. Despite both FcγRIIIa allotypes having very similar levels of ADCC activity, FcγRIIIa-158F had more binding activity. For FcγRIIIb-NA1 and FcγRIIIb-NA2, receptor binding patterns were similar to those for FcγRIIIa. Most of the afucosylated glycans had higher binding activities than the fucosylated glycans (Figure 4G-H). However, as a group, the fucosylated glycans of FcγRIIIb had higher binding than those of FcγRIIIa. In both FcγRIIIa and FcγRIIIb, galactosylation tended to increase binding in afucosylated glycans.

Next, we fit the inferred and measured binding activities to assess the contributions we calculated for each glycan. Following the same method described for ADCC deconvolution, we multiplied the mixture matrix by the inferred β vector for receptor binding then compared these values to the measurements reported in Dekkers et al. (Figure 5). For the FcγRII allotypes, the inferred binding activities were excellent fits for the measured values. For FcγRI and FcγIII, the inferred activities showed small deviations from the measured activities. This was likely due to grouping certain glycans to share the same activity. Nevertheless, the fits for FcγRI and FcγIII were still very good for most of the mixtures.

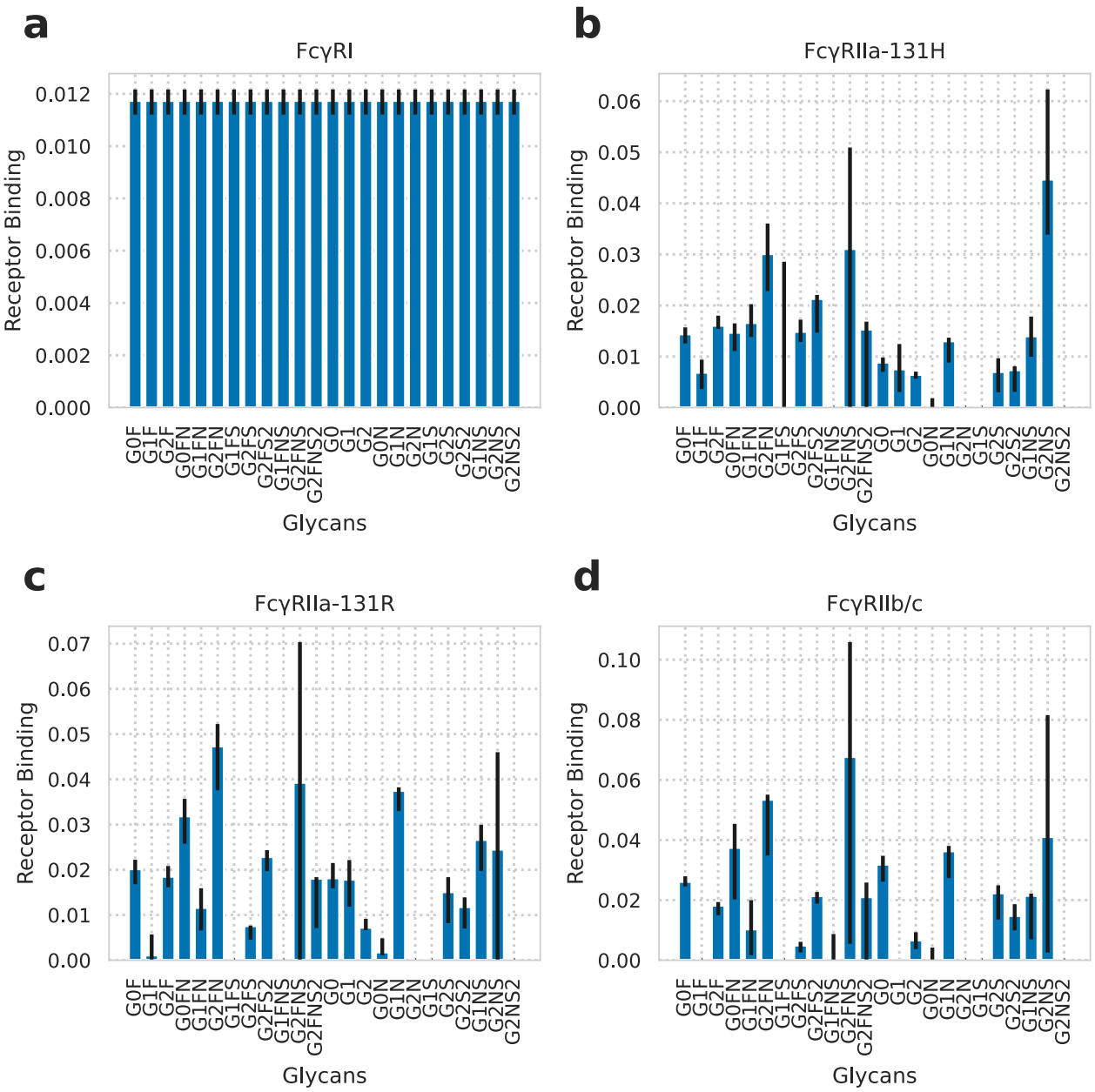

Figure 4: Deconvolution of Receptor Binding. Inferred receptor binding of each pure glycan species to FcγRI (A), FcγRIIa-131H (B), FcγRIIa-131R (C), FcγRIIb/c (D), FcγRIIIa-158F (E), FcγRIIIa-158V (F), FcγRIIIb-NA1 (G), and FcγRIIIb-NA2 (H). Measurements of receptor binding in glycan mixtures were taken from Dekkers et al. (Figure 8). Error bars were obtained with bootstrapping and represent the 67% confidence intervals.

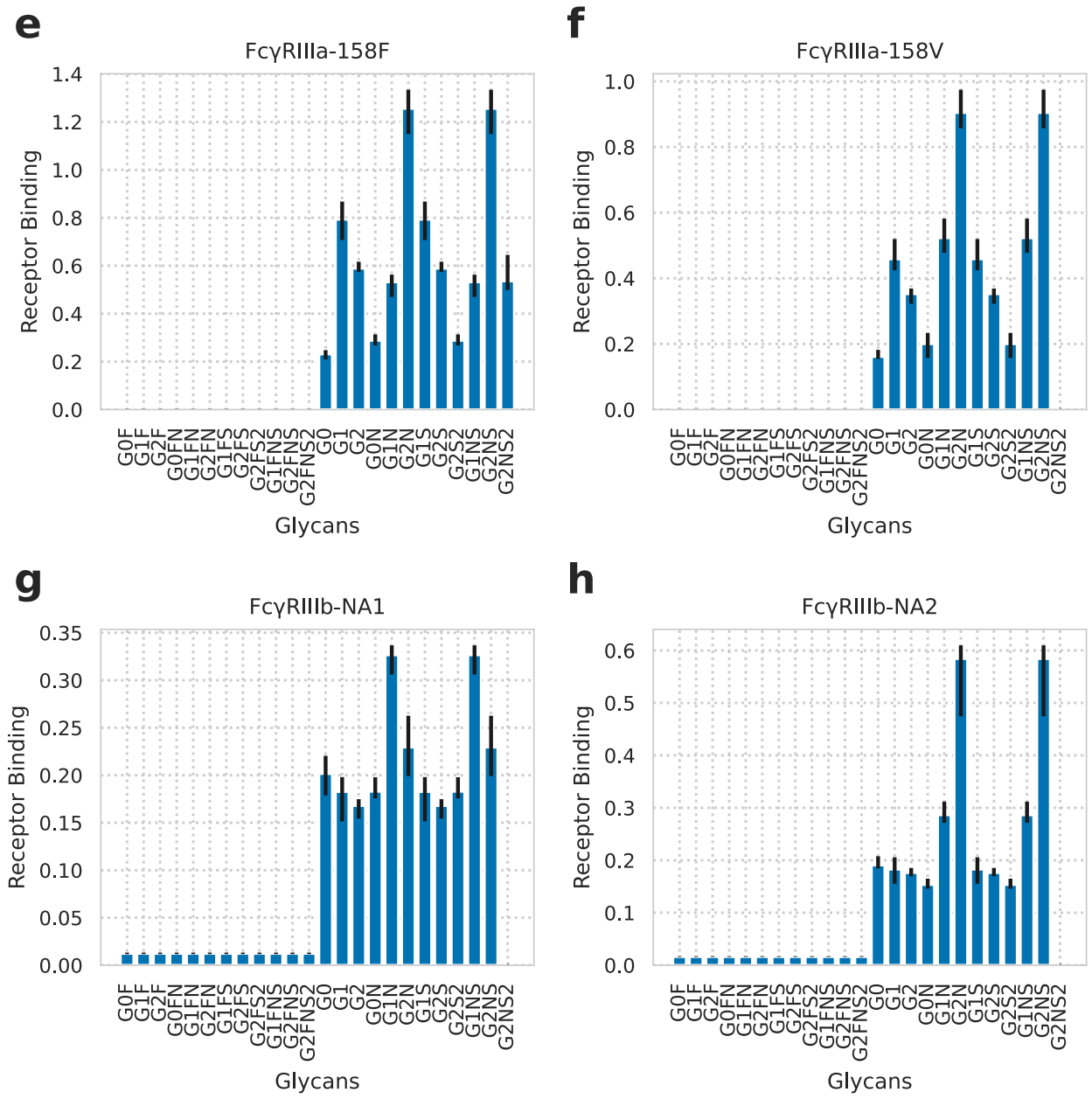

Figure 4 continued

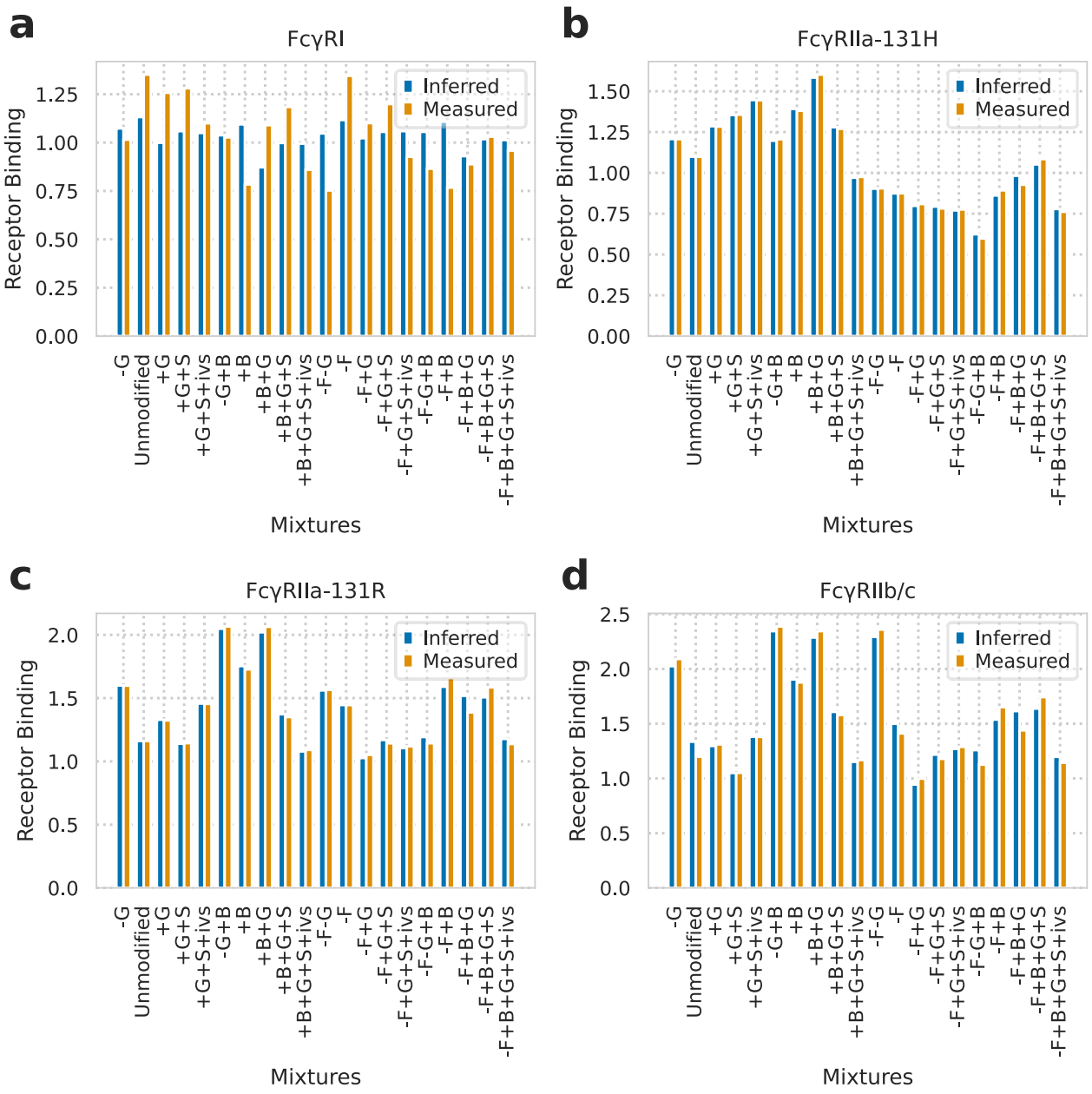

Figure 5: Fitting of measured and inferred receptor binding. Grouped bar plot comparing the inferred and measured receptor binding of 20 mixtures to FcγRI (A), FcγRIIa-131H (B), FcγRIIa-131R (C), FcγRIIb/c (D), FcγRIIIa-158F (E), FcγRIIIa-158V (F), FcγRIIIb-NA1 (G), and FcγRIIIb-NA2 (H). Measured values were taken from Dekkers et al. (Figure 8). Fit values were calculated using the previous receptor binding deconvolution.

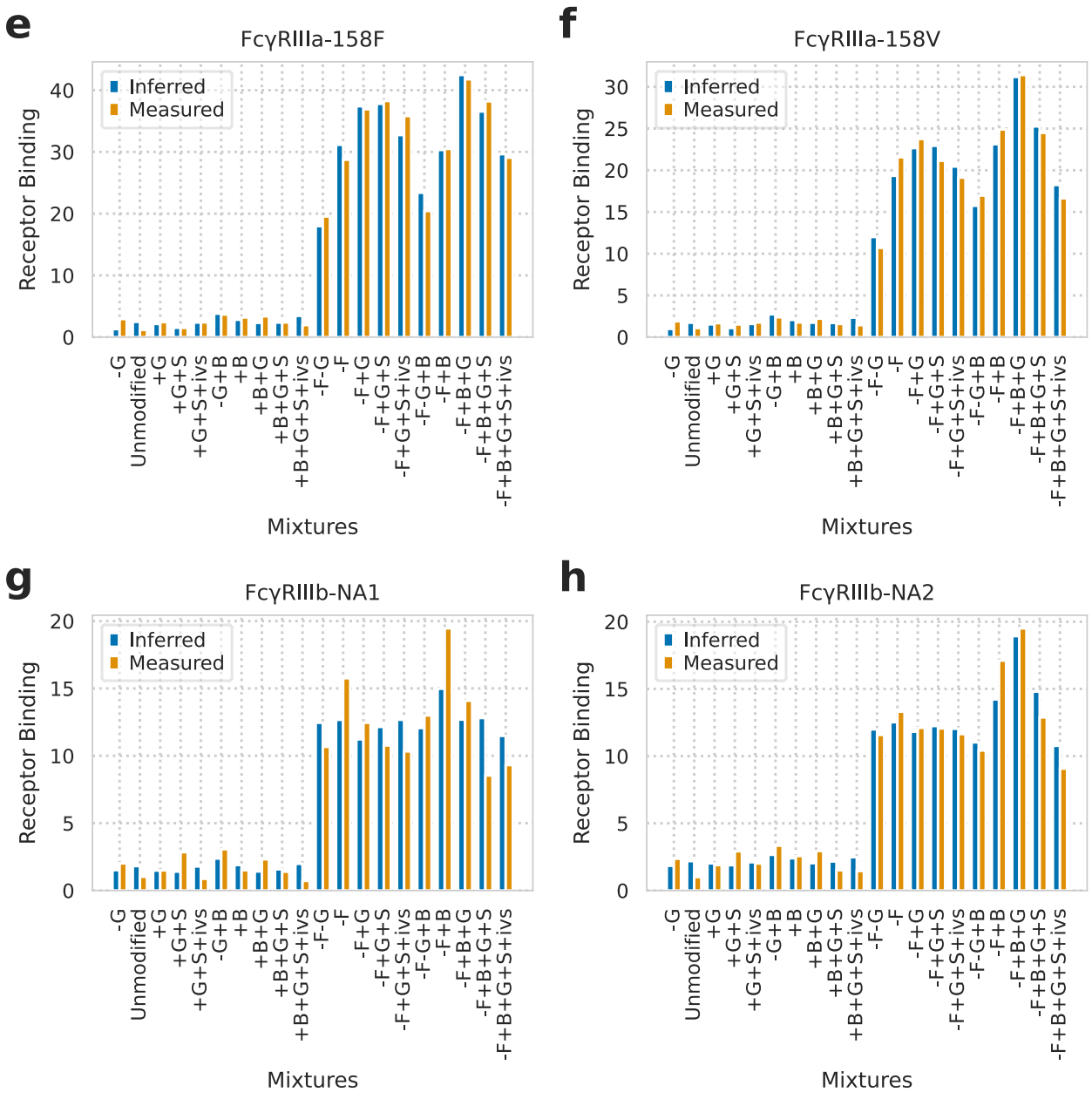

Figure 5 continued

Cross-Validation

We performed cross-validation to determine how well the deconvolution predicts ADCC and receptor binding activities of unseen mixtures. Plotting measured activities by inferred activities revealed that inferred ADCC is an excellent predictor of actual, measured ADCC

(Figure 6). The points for each mixture lie very close to the line y=x, which represents perfect predictive accuracy. For receptor binding, the FcγRI and FcγRIII cross-validation revealed good predictive accuracy, although not as good as the previous ADCC cross-validation (Figure 7). The FcγRII cross-validation showed lower predictive accuracy compared to FcγRI and FcγRIII. Because glycan grouping was used for FcγRI and FcγRIII but not FcγRII, the increased predictive accuracy of FcγRI and FcγRIII was likely a result of including those groups.

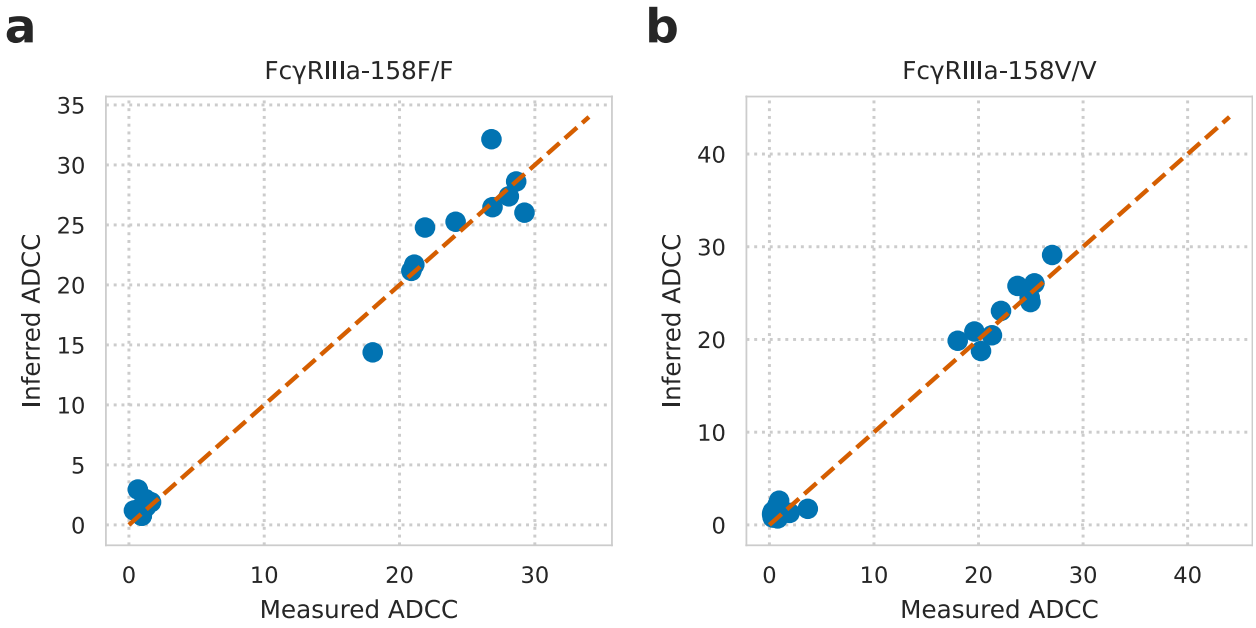

Figure 6: ADCC Cross-Validation. Points represent ADCC activities of 20 anti-D mixtures as a function of measured and inferred ADCC activities. Inferred activities were calculated by sequentially removing one mixture, performing deconvolution with the remaining 19 mixtures, and reconstructing the activity of the removed mixture from the deconvolution results. The dashed line y=x represents perfect predictive accuracy, meaning that inferred ADCC activities exactly match measured activities.

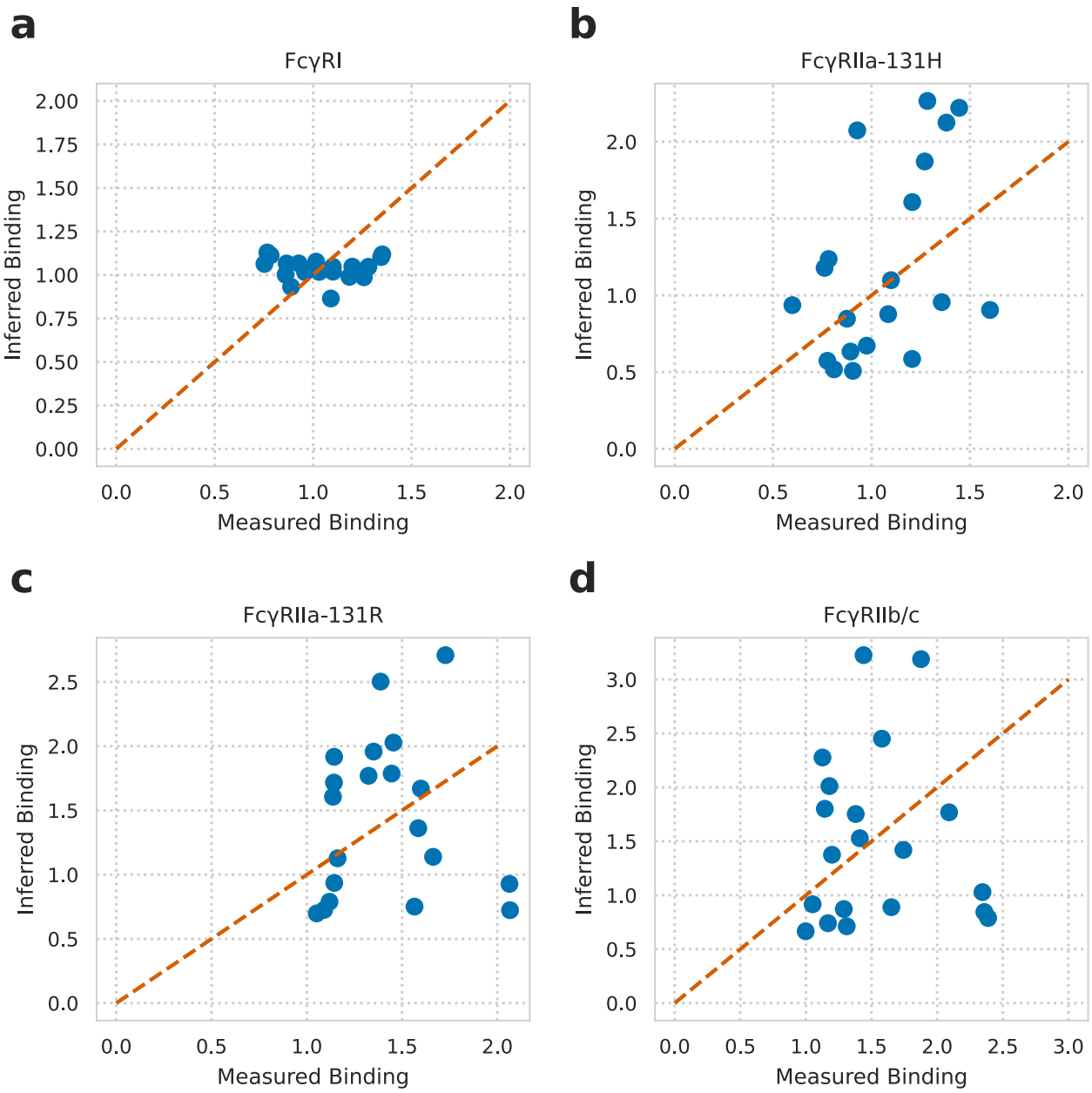

Figure 7: Receptor Binding Cross-Validation. Points represent receptor binding activities of 20 anti-D mixtures as a function of measured and inferred binding. Inferred activities were calculated by sequentially removing one mixture, performing deconvolution with the remaining 19 mixtures, and reconstructing the activity of the removed mixture from the deconvolution results. The dashed line y=x represents perfect predictive accuracy.

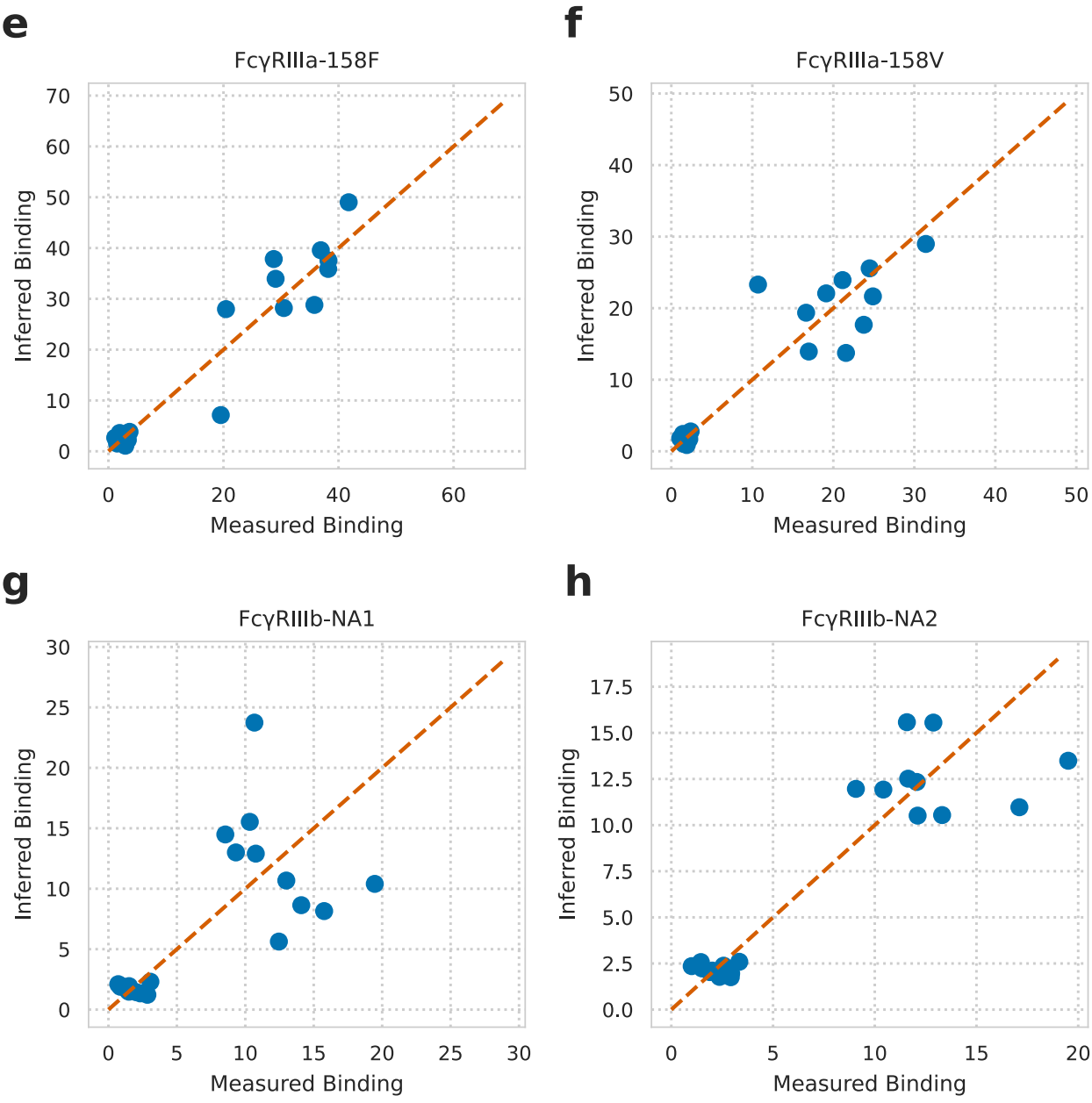

Figure 7 continued

DISCUSSION

In the first deconvolution of ADCC using mixtures of anti-D IgG, our results showed that the afucosylated glycans had higher inferred ADCC activities than the fucosylated ones (Figure 2, Table 1). This finding is supported by previous research, which has shown that afucosylated antibodies can be used as therapeutic treatments by increasing ADCC [Iida et al., 2006; Satoh et al., 2006]. In addition, our comparisons of the inferred and measured activities of ADCC and receptor binding further supported the deconvolution results. The fitted outcomes were very similar to those measured experimentally and only exhibited minor deviations (Figures 3, 5). Furthermore, cross-validation showed very good predictive accuracy for ADCC in both FcγRIIIa allotypes as well as for receptor binding in FcγRI and FcγRIII (Figures 6, 7).

The deconvolution of receptor binding activity revealed similar trends in all four FcγRIII allotypes (Figure 4). Because the ADCC experiments used NK cells from FcγRIIIa-158F/F and FcγRIIIa-158V/V donors, the deconvolution supports that afucosylation in these two allotypes contributes to higher levels of both ADCC and receptor binding activity. Afucosylation is likely increasing receptor binding directly, which then increases the downstream ADCC response. Interestingly, FcγRIIIa-158F had more binding activity than FcγRIIIa-158V although the two types had very similar levels of ADCC (Figures 2, 4). This result suggests that FcγRIIIa-158F may induce ADCC more efficiently and thus requires less binding activity to achieve a similar level of ADCC.

Among the afucosylated glycans of the FcγRIII allotypes, those that had the highest binding activities also tended to be galactosylated (G1 or G2, compared to non-galactosylated G0) (Figure 4). This is consistent with the PCA scores for each mixture, which showed a separation between the galactosylated and non-galactosylated mixtures along component 2

(Figure 1A). Therefore, the variance explained by component 2 may be mostly due to galactosylation. In addition, the clustering of fucosylated mixture scores suggests that the variance explained by component 1 may be mostly due to fucosylation. This is probable because fucosylation seems to have the most significant impact on glycan activities.

For future directions, we plan to apply deconvolution to complement activation, which was measured using the anti-TNP mixtures in Dekkers et al. (Figure 10). Understanding how different glycans contribute to complement activation as well as to ADCC and receptor binding will provide a more complete picture of the complex mechanisms mediated by Fcγ receptors. We also plan to perform experiments for further validation of our computational techniques. Specifically, we are interested in expressing certain glycans in their pure forms to investigate whether our inferences of their individual activities are supported experimentally. Because engineering specific glycan forms is very difficult, there is limited data on the effects of glycan variation in the Fc region of IgG. As glycan-engineering methods advance, more data will become available to study a wider variety of Fc-mediated immune responses using deconvolution.

Moreover, our deconvolution methods can provide important information for building computational models of IgG effector response by revealing the influence of specific glycans on different effector responses. While we studied how glycans can modulate ADCC through interaction with FcγRIIIa allotypes, future studies may investigate the effects of glycan variation on effector responses modulated by the FcγRI and FcγRII allotypes. In addition, the experiments from Dekkers et al. used antibodies specific for either the human RhD (anti-D) or 2,4,6-trinitrophenyl hapten (anti-TNP) antigens. Performing experiments using antibodies specific for

different, clinically significant antigen targets may also be helpful in discovering new therapeutic treatments.

In this study, we used deconvolution to better understand mixtures of IgG glycans. However, there are many other biological problems to which this technique can be extremely informative. Deconvolution has already been applied to mixtures of proteases and cell types, but it can be applied to many other problems involving species that are difficult to isolate and study experimentally, in their pure forms [Miller et al., 2011; Wang et al., 2019; Avila Cobos et al., 2020].

TABLE 1 | Comprehensive list of glycopeptide degrees of complex glycans found in the glyco-engineered IgG1 batches of anti-D and anti-TNP specificity.

name	glyco-engineering					relative abundance glycopeptides*																								
anti-D	2FF (-F)	2FG (-G)	GNT3 (+B)	B4GALT1/D-galactose (+G)	ST6GALT (+S)	in vitro sialylation (+ivs)	G0F	G1F	G2F	G0FN	G1FN	G2FN	G1FS	G2FS	G2FS2	G1FNS	G2FNS	G2FNS2	G0	G1	G2	G0N	G1N	G2N	G1S	G2S	G2S2	G1NS	G2NS	G2NS2
-G	-	+	-	-	-	-	72.7	12.7	1.2	1.6	0.4	0.0	0.2	0.4	0.1	0.0	0.0	0.0	0.9	0.8	0.1	0.1	0.1	0.0	0.1	0.0	0.0	0.0	0.0	0.0
Unmodified	-	-	-	-	-	-	37.5	37.7	9.8	1.8	2.6	0.4	0.7	1.5	0.7	0.1	0.1	0.0	0.1	0.8	0.7	0.2	0.3	0.1	0.6	0.3	0.2	0.1	0.0	0.1
+G	-	-	+	-	-	-	2.3	7.6	54.6	0.1	1.0	0.9	0.1	11.7	4.0	0.2	0.1	0.0	0.0	0.1	0.4	0.0	0.0	0.5	0.4	0.8	0.2	0.0	0.1	0.0
+G+S	-	-	-	+	+	-	4.2	10.0	14.2	0.1	0.5	0.3	3.2	35.0	19.9	0.5	0.3	0.1	0.1	0.1	0.2	0.0	0.0	0.1	0.1	0.5	0.3	0.0	0.3	0.2
+G+S+ivs	-	-	-	+	+	+	3.8	2.9	0.2	0.2	0.1	0.1	10.4	14.2	51.8	0.7	0.2	0.6	0.3	0.4	0.1	0.1	0.0	0.0	0.5	0.8	1.4	0.2	0.1	0.3
-G+B	-	+	+	-	-	-	11.5	8.8	9.3	46.2	5.7	0.1	0.0	0.0	0.0	0.1	0.0	0.0	0.5	0.8	2.8	1.2	1.2	0.1	0.1	0.0	0.0	0.0	0.0	0.0
+B	-	-	+	-	-	-	4.8	8.5	11.3	26.1	33.0	3.1	0.2	0.5	0.0	1.1	0.6	0.1	0.1	0.3	2.0	0.2	0.4	0.4	0.1	0.1	0.0	0.2	0.1	0.0
+B+G	-	-	+	+	-	-	1.0	2.9	13.0	1.4	16.5	26.4	0.2	3.2	0.8	0.4	4.1	1.9	0.0	0.1	0.4	0.0	0.1	0.6	0.1	0.3	0.1	0.3	0.4	0.1
+B+G+S	-	-	+	+	+	-	2.4	5.1	5.4	2.6	10.9	5.6	1.7	12.1	7.1	12.4	6.9	9.9	0.2	0.2	0.6	0.0	0.1	0.3	0.1	0.3	0.2	0.2	0.5	0.2
+B+G+S+ivs	-	-	+	+	+	+	2.3	1.8	1.2	2.4	0.7	0.2	5.0	5.4	17.8	21.7	0.6	20.3	0.3	0.3	0.7	0.2	0.1	0.0	0.3	0.4	0.7	0.9	0.7	0.7
-F-G	+	+	-	-	-	-	20.4	4.9	1.2	0.6	0.3	0.1	0.1	0.7	0.2	0.1	0.0	0.0	52.7	6.1	0.4	0.8	0.2	0.0	0.1	0.1	0.1	0.0	0.1	0.0
-F	+	-	-	-	-	-	11.4	13.3	3.9	0.5	0.8	0.1	0.3	0.6	0.5	0.1	0.0	0.1	30.6	23.5	5.1	1.0	1.2	0.2	0.5	0.7	0.4	0.1	0.1	0.1
-F+G	+	-	-	+	-	-	0.6	2.2	15.7	0.5	0.2	0.2	0.1	3.3	1.5	0.0	0.0	0.0	2.4	7.4	42.7	0.1	0.6	0.6	0.2	6.4	2.3	0.1	0.0	0.0
-F+G+S	+	-	-	+	+	-	1.5	3.0	3.0	0.1	0.1	0.1	1.3	8.9	5.3	0.1	0.1	0.0	5.6	11.9	6.8	0.1	0.3	0.2	6.0	24.2	10.8	0.2	0.2	0.1
-F+G+S+ivs	+	-	-	+	+	+	1.5	1.0	0.4	0.1	0.1	0.1	3.3	2.8	12.6	0.2	0.2	0.0	5.2	4.3	0.2	0.1	0.2	0.2	14.0	11.4	31.5	0.3	0.3	0.2
-F-G+B	+	+	+	-	-	-	4.3	3.0	2.3	16.1	2.6	0.1	0.0	0.0	0.1	0.0	0.0	0.0	9.6	5.8	7.9	34.9	2.9	0.1	0.0	0.0	0.0	0.1	0.0	0.1
-F+B	+	-	+	-	-	-	1.8	3.0	2.5	8.8	11.5	1.1	0.1	0.2	0.1	0.5	0.3	0.1	4.3	5.6	8.4	24.4	18.9	1.4	0.1	0.2	0.0	0.7	0.3	0.1
-F+B+G	+	-	+	+	-	-	0.4	1.2	5.0	0.7	5.6	9.1	0.3	1.1	0.4	0.2	1.7	0.8	1.0	2.5	10.5	1.3	14.8	16.4	0.2	1.8	0.5	0.3	2.5	0.9
-F+B+G+S	+	-	+	+	+	-	0.7	1.6	1.9	1.0	3.8	2.4	0.5	4.4	2.5	3.5	2.5	3.8	2.1	4.1	3.6	2.2	9.0	3.5	1.8	9.7	4.5	8.6	4.1	4.9
-F+B+G+S+ivs	+	-	+	+	+	+	0.8	0.7	0.4	0.9	0.3	0.5	1.5	1.8	6.0	7.2	0.3	7.5	2.0	1.7	1.0	2.0	0.7	0.1	4.3	5.2	12.2	17.1	0.7	11.4

(*Continued*)

Table 2: Anti-D and Anti-TNP Mixture Components [Dekkers et al., 2017]

TABLE 1 | Continued

anti-TNP																													
-G	-	+	-	-	-	-	63.5	9.0	0.0	0.0	0.0	0.0	0.0	0.0	0.0	0.0	0.0	0.0	3.0	2.2	0.0	0.0	0.0	0.0	0.0	0.0	0.0	0.0	0.0	0.0
Unmodified	-	-	-	-	-	-	59.6	22.5	3.0	1.8	0.9	0.1	0.6	0.5	0.3	0.1	0.1	0.1	0.6	1.4	0.5	0.1	0.1	0.0	0.3	0.1	0.0	0.1	0.0	0.1
+G	-	-	-	+	-	-	3.5	8.6	54.4	0.1	0.6	0.5	0.1	11.8	3.1	0.1	0.0	0.0	0.1	0.1	0.3	0.0	0.0	0.2	1.2	0.5	0.1	0.0	0.0	0.0
+G+S	-	-	-	+	+	-	4.9	9.7	11.5	0.1	0.3	0.2	3.8	31.1	20.4	0.3	0.2	0.1	0.0	0.2	0.2	0.0	0.1	0.1	0.2	0.5	0.3	0.1	0.2	0.2
+G+S+ivs	-	-	-	+	+	+	4.1	2.5	0.2	0.2	0.2	0.2	10.3	11.4	51.5	0.4	0.2	0.3	0.3	0.3	0.2	0.1	0.1	0.1	0.2	0.4	0.5	0.3	0.1	0.4
-G+B	-	+	+	-	-	-	8.8	11.0	12.8	38.5	5.3	0.1	0.0	0.1	0.0	0.1	0.0	0.0	0.4	1.0	4.7	0.6	0.9	0.2	0.1	0.0	0.0	0.0	0.0	0.0
+B	-	-	+	-	-	-	10.5	12.3	12.8	32.4	16.9	1.1	0.1	0.2	0.0	0.6	0.2	0.1	0.1	0.6	3.2	0.2	0.7	0.3	0.2	0.1	0.0	0.1	0.0	0.0
+B+G	-	-	+	+	-	-	0.7	2.0	10.6	0.9	16.2	33.0	0.1	2.4	0.5	0.3	4.2	1.5	0.0	0.1	0.3	0.1	0.2	0.3	0.0	0.1	0.0	0.1	0.2	0.1
+B+G+S	-	-	+	+	+	-	2.0	4.4	5.1	2.3	10.1	5.3	1.6	10.9	6.4	12.2	6.5	9.7	0.4	0.5	0.9	0.0	0.1	0.3	0.2	1.5	0.6	0.2	0.5	0.2
+B+G+S+ivs	-	-	+	+	+	+	2.1	1.6	1.3	2.3	0.5	0.1	4.9	4.6	17.9	21.0	0.5	19.2	0.5	0.4	0.6	0.1	0.1	0.0	0.6	0.9	1.9	0.2	0.7	0.3
-F-G	+	+	-	-	-	-	20.7	7.0	0.8	0.4	0.2	0.0	0.1	0.1	0.1	0.0	0.0	0.0	44.8	10.2	0.8	0.6	0.3	0.0	0.2	0.1	0.1	0.0	0.0	0.1
-F	+	-	-	-	-	-	15.3	7.7	1.2	0.4	0.3	0.1	0.2	0.2	0.3	0.1	0.1	0.1	46.1	14.6	1.6	1.0	0.5	0.1	0.4	0.3	0.2	0.1	0.1	0.1
-F+G	+	-	-	+	-	-	1.8	4.3	21.0	0.3	0.3	0.3	0.1	4.8	2.5	0.1	0.1	0.1	3.5	6.8	29.5	0.1	0.4	0.3	0.2	4.7	1.9	0.1	0.0	0.0
-F+G+S	+	-	-	+	+	-	1.1	2.6	3.8	0.1	0.2	0.2	1.0	9.4	5.0	0.2	0.2	0.1	4.1	8.9	8.9	0.1	0.3	0.2	3.8	26.7	11.5	0.3	0.2	0.1
-F+G+S+ivs	+	-	-	+	+	+	1.3	0.9	0.3	0.1	0.1	0.1	3.1	3.9	16.7	0.5	0.2	0.4	3.9	3.2	0.1	0.1	0.1	0.1	9.5	12.5	32.1	0.3	0.1	0.2
-F-G+B	+	+	+	-	-	-	3.5	3.9	3.2	16.1	2.6	0.1	0.0	0.0	0.0	0.1	0.0	0.0	7.3	6.9	10.9	27.9	2.8	0.1	0.0	0.0	0.0	0.1	0.0	0.1
-F+B	+	-	+	-	-	-	3.2	4.5	2.7	9.3	10.2	0.9	0.1	0.1	0.1	0.3	0.2	0.0	9.0	8.5	7.7	20.7	13.7	1.1	0.2	0.2	0.1	0.4	0.2	0.1
-F+B+G	+	-	+	+	-	-	0.4	1.0	4.2	0.8	5.5	9.1	0.2	0.9	0.4	0.2	1.8	0.9	1.0	2.1	9.2	1.5	13.4	15.8	0.1	1.5	0.5	0.3	2.8	1.0
-F+B+G+S	+	-	+	+	+	-	0.6	1.5	1.8	0.9	3.5	2.3	0.5	4.0	2.4	3.3	2.3	3.5	2.2	4.3	3.9	2.4	9.1	3.6	1.9	9.2	4.4	9.0	4.0	5.0
-F+B+G+S+ivs	+	-	+	+	+	+	0.7	0.6	0.4	0.9	0.3	0.5	1.6	1.7	6.2	7.0	0.2	7.5	2.2	1.8	1.1	2.2	0.8	0.1	4.6	4.9	11.6	16.8	0.6	11.0
							Complex glycans																							

2FF, 0.4 mM 2-deoxy-2-fluoro-L-fucose; 2FG, 1 mM 2-deoxy-2-fluoro-D-galactose; GNT3, co-transfection of 1% GNT3 vector; B4GALT1/D-galactose, co-transfection of 1% B4GALT1 vector and addition of 5 mM D-galactose; ST6GALT, co-transfection of 2.5% ST6GALT vector; in vitro sialylation, treatment of sample with recombinant ST6GALT and CMP-NANA; G, number of galactoses; F, presence of a core fucose; N, presence of a bisecting N-acetylglucosamine; S, number of N-acetylneuraminic (sialic) acids.

These resulted in significantly different derived glycosylation traits (fucosylation, bisection, galactosylation, sialylation, high-mannose, hybrid-type), which are calculated from the relative abundances of individual N-glycans. The shading of cells indicates, for each glycoform the lowest to highest abundance of glycopeptides, respectively, from light to dark.

[a]*For complex immunoglobulin G glycans, we use a nomenclature which assumes structural knowledge of the glycans based on literature.*

Table 2 continued

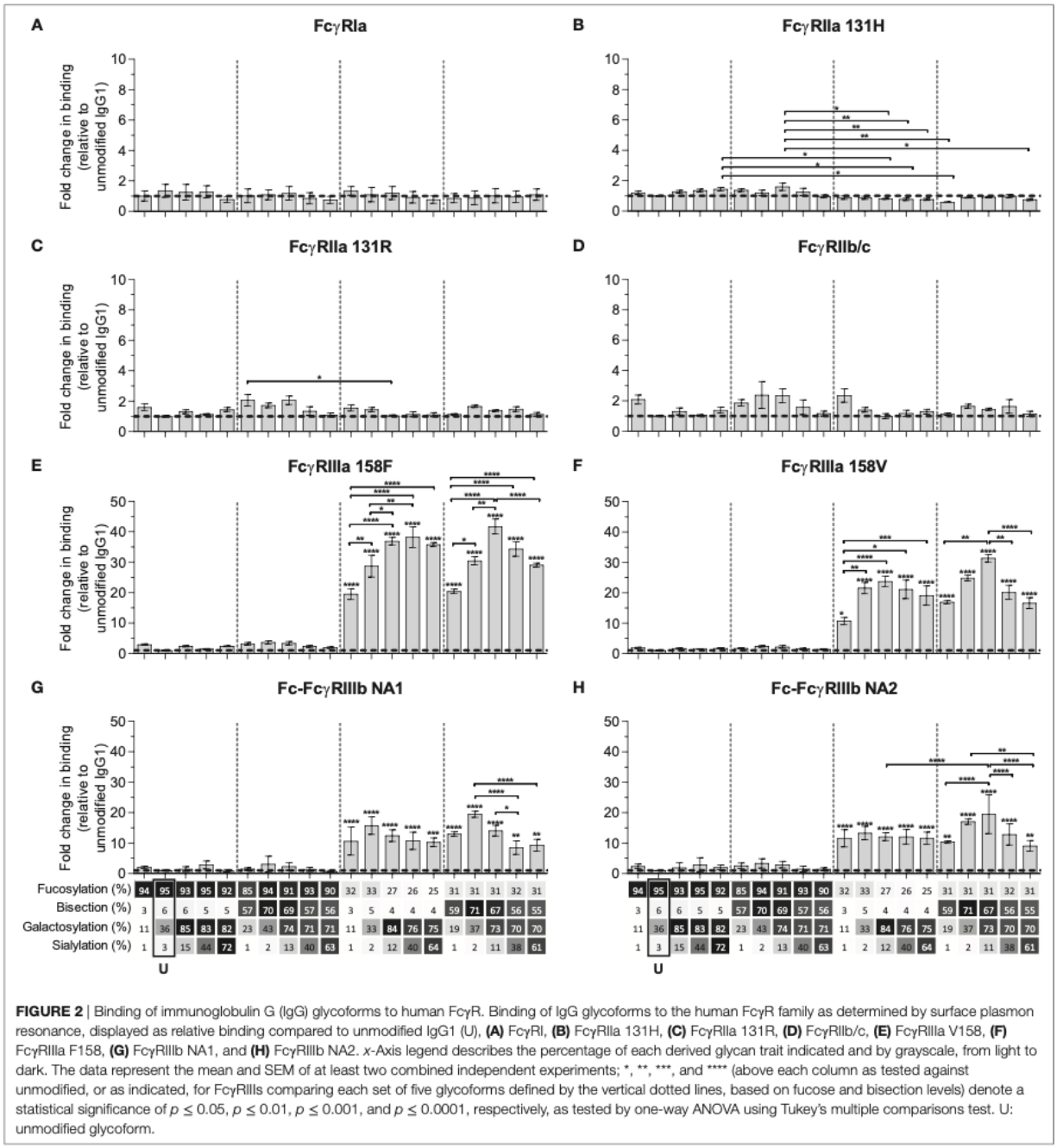

FIGURE 2 | Binding of immunoglobulin G (IgG) glycoforms to human FcγR. Binding of IgG glycoforms to the human FcγR family as determined by surface plasmon resonance, displayed as relative binding compared to unmodified IgG1 (U), **(A)** FcγRI, **(B)** FcγRIIa 131H, **(C)** FcγRIIa 131R, **(D)** FcγRIIb/c, **(E)** FcγRIIIa V158, **(F)** FcγRIIIa F158, **(G)** FcγRIIIb NA1, and **(H)** FcγRIIIb NA2. *x*-Axis legend describes the percentage of each derived glycan trait indicated and by grayscale, from light to dark. The data represent the mean and SEM of at least two combined independent experiments; *, **, ***, and **** (above each column as tested against unmodified, or as indicated, for FcγRIIIs comparing each set of five glycoforms defined by the vertical dotted lines, based on fucose and bisection levels) denote a statistical significance of $p \leq 0.05$, $p \leq 0.01$, $p \leq 0.001$, and $p \leq 0.0001$, respectively, as tested by one-way ANOVA using Tukey's multiple comparisons test. U: unmodified glycoform.

Figure 8: Measurements of FcγR binding to IgG1 [Dekkers et al., 2017]

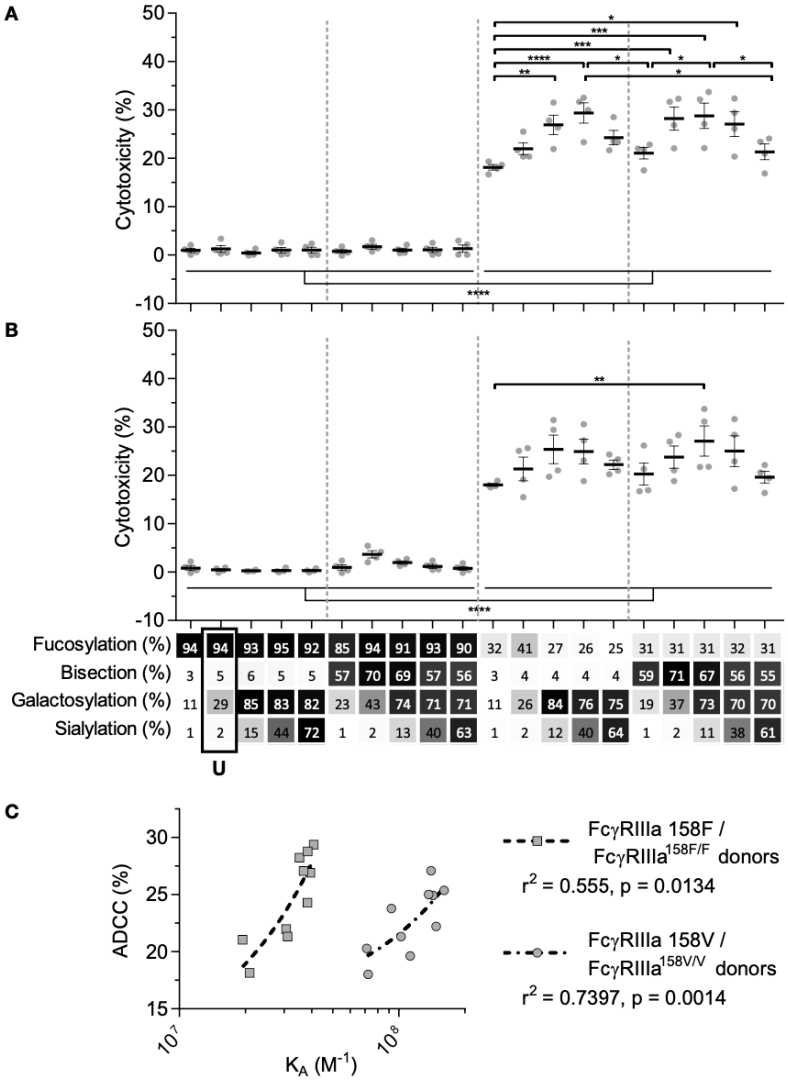

FIGURE 3 | NK cell-mediated antibody-dependent cellular cytotoxicity (ADCC) of anti-D glycoform opsonized red blood cell. ADCC mediated by NK cells from monozygotic FcγRIIIA$^{158F/F}$ donors **(A)**, or monozygotic FcγRIIIA$^{158V/V}$ donors **(B)**, data represent the mean and SEM of four combined independent experiments; *, **, ***, and **** denote a statistical significance of $p \leq 0.05$, $p \leq 0.01$, $p \leq 0.001$, and $p \leq 0.0001$, respectively, as tested by one-way ANOVA using Tukey's multiple comparisons test. *x*-Axis legend describes the percentage of each derived glycan trait indicated and by grayscale, from light to dark. **(C)** Correlation between K_A of FcγRIIIa F158 or FcγRIIIa V158 binding of hypo-fucosylated glycoforms and ADCC activity of FcγRIIIA$^{158F/F}$ or FcγRIIIA$^{158V/V}$ donors, respectively. r^2 and p value shown where obtained using a two-tailed Pearson's correlation. U: unmodified glycoform.

Figure 9: Measurements of antibody-dependent cellular cytotoxicity (ADCC) [Dekkers et al., 2017]

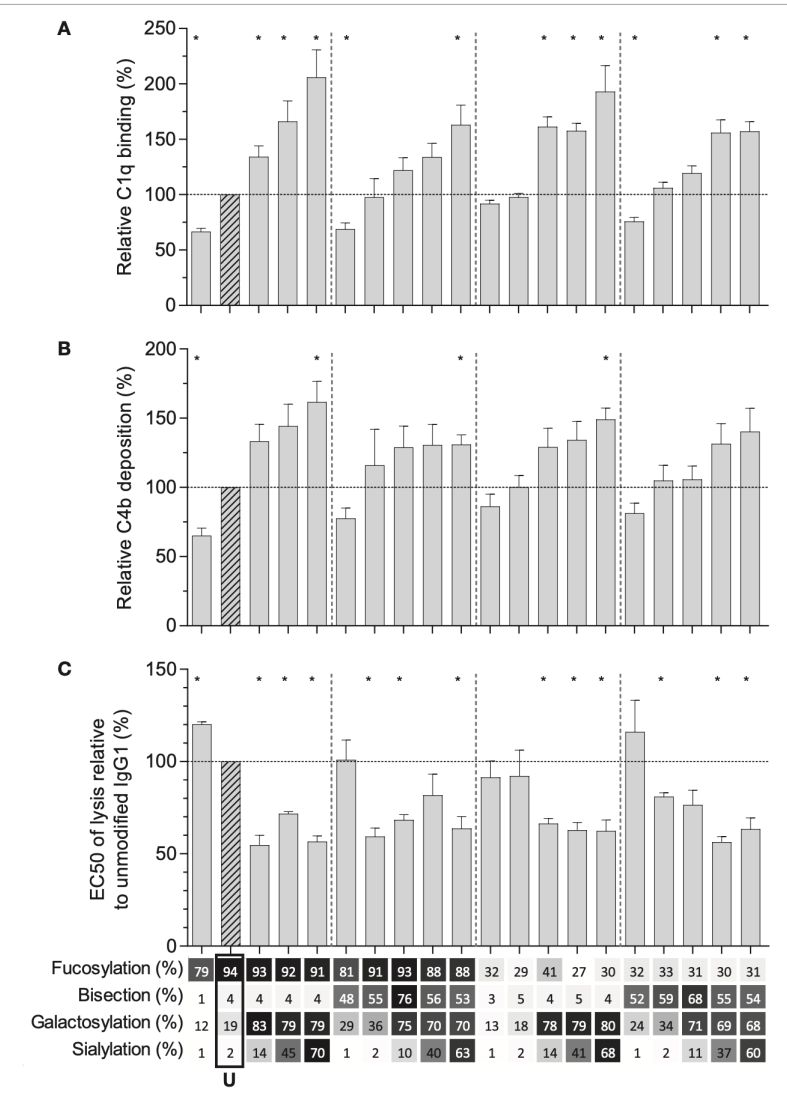

FIGURE 4 | Complement activation by glyco-engineered anti-TNP IgG1. Relative **(A)** binding of C1q ($n = 4$) and **(B)** C4 deposition as determined by ELISA ($n = 4$), **(C)** complement-mediated lysis of aTNP opsonized red blood cells ($n = 3$). Data represent the mean and SEM of combined independent experiments; *denotes a statistical significance of $p \leq 0.05$, as tested by a one-sample *t*-test against a theoretical mean of 100 (%). *x*-Axis legend describes the percentage of each derived glycan trait indicated and by grayscale, from light to dark. U: unmodified glycoform.

Figure 10: Measurements of complement activation [Dekkers et al., 2017]

REFERENCES

Avila Cobos, F., Alquicira-Hernandez, J., Powell, J.E., Mestdagh, P., & De Preter, K. (2020). Benchmarking of cell type deconvolution pipelines for transcriptomics data. *Nature Communications*, 11(5650). https://doi.org/10.1038/s41467-020-19015-1

Bournazos, S., Gupta, A., & Ravetch, J.V. (2020). The role of IgG Fc receptors in antibody-dependent enhancement. *Nature Reviews Immunology*, *20*(10), 633-643. https://doi.org/10.1038/s41577-020-00410-0

Bournazos, S., Corti, D., Virgin, H.W., & Ravetch, J.V. (2020). Fc-optimized antibodies elicit CD8 immunity to viral respiratory infection. *Nature*, *588*(7838), 485-490. https://doi.org/10.1038/s41586-020-2838-z

Dekkers, G., Treffers, L., Plomp, R., Bentlage, A.E.H., De Boer, M., Koeleman, C.A.M., Lissenberg-Thunnissen, S.N., Visser, R., Brouwer, M., Mok, J.Y., Matlung, H., van den Berg, T.K., van Esch, W.J.E., Kuijpers, T.W., Wouters, D., Rispens, T., Wuhrer, M. & Vidarsson, G. (2017). Decoding the human immunoglobulin G-glycan repertoire reveals a spectrum of Fc-receptor-and complement-mediated-effector activities. *Frontiers in immunology*, *8*(877). https://doi.org/10.3389/fimmu.2017.00877

Duchemin, A.M., Ernst, L.K. & Anderson, C.L. (1994). Clustering of the high affinity Fc receptor for immunoglobulin G (FcγRI) results in phosphorylation of its associated γ-chain. *The Journal of Biological Chemistry, 269*(16), 12111–12117.

Iida, S., Misaka, H., Inoue, M., Shibata, M., Nakano, R., Yamane-Ohnuki, N., Wakitani, M., Yano, K., Shitara, K., & Satoh, M. (2006). Nonfucosylated Therapeutic IgG1 Antibody Can Evade the Inhibitory Effect of Serum Immunoglobulin G on Antibody-Dependent Cellular Cytotoxicity through its High Binding to FcγRIIIa. *Clinical Cancer Research*,

12(9), 2879-2887. https://doi.org/10.1158/1078-0432.CCR-05-2619

Levin, A., Weiss, Y., Durand, F., & Freeman, W.T. (2009). Understanding and evaluating blind deconvolution algorithms. *2009 IEEE Conference on Computer Vision and Pattern Recognition*, 1964-1971, https://doi.org/10.1109/CVPR.2009.5206815

Li, T., DiLillo, D.J., Bournazos, S., Giddens, J.P., Ravetch, J.V., & Wang, L.X. (2017). Modulating IgG effector function by Fc glycan engineering. *Proceedings of the National Academy of Sciences*, *114*(13), 3485-3490. https://doi.org/10.1073/pnas.1702173114

Miller, M.A., Barkal, L., Jeng, K., Herrlich, A., Moss, M., Griffith, L.G., & Lauffenburger, D.A. (2011). Proteolytic Activity Matrix Analysis (PrAMA) for simultaneous determination of multiple protease activities. *Integrative Biology*, *3*(4), 422-438. https://doi.org/10.1039/c0ib00083c

Satoh, M., Iida, S., & Shitara, K. (2006). Non-fucosylated therapeutic antibodies as next-generation therapeutic antibodies. *Expert Opinion on Biological Therapy, 6*(11), 1161-1173. https://doi.org/10.1517/14712598.6.11.1161

Smith, S.W. (1997). *The Scientist and Engineer's Guide to Digital Signal Processing*. California Technical Publishing.

van Erp, E.A., Luytjes, W., Ferwerda, G., & van Kasteren, P.B. (2019). Fc-Mediated Antibody Effector Functions During Respiratory Syncytial Virus Infection and Disease. *Frontiers in Immunology, 20*(548). https://doi.org/10.3389/fimmu.2019.00548

Von Holle, T.A., & Moody, M.A. (2019). Influenza and Antibody-Dependent Cellular Cytotoxicity. *Frontiers in Immunology, 10*(1457). https://doi.org/10.3389/fimmu.2019.01457

Wang, X., Park, J., Susztak, K., Zhang, N.R., & Li, M. (2019). Bulk tissue cell type

deconvolution with multi-subject single-cell expression reference. *Nature Communications*, 10(380). https://doi.org/10.1038/s41467-018-08023-x

Zahavi, D., AlDeghaither, D., O'Connell, A., & Weiner, L.M. (2018). Enhancing antibody-dependent cell-mediated cytotoxicity: a strategy for improving antibody-based immunotherapy. *Antibody Therapeutics, 1*(1), 7-12. https://doi.org/10.1093/abt/tby002